Automation in Construction 151 (2023) 104869

Contents lists available at ScienceDirect

Automation in Construction

journal homepage: www.elsevier.com/locate/autcon

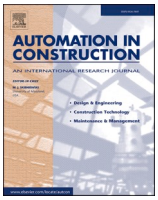

Formwork pressure prediction in cast-in-place self-compacting concrete using deep learning

Yaser Gamil [a,*], Jonny Nilimaa [a], Taufik Najeh [b], Andrzej Cwirzen [a]

[a] Building Materials, Department of Civil, Environmental and Natural Resources Engineering, Lulea University of Technology, 97187 Luleå, Sweden
[b] Operation, Maintenance and Acoustics, Department of Civil, Environmental and Natural Resources Engineering Lulea University of Technology, 97187 Luleå, Sweden

ARTICLE INFO

Keywords:
Formwork pressure
Casting in place
Self-compacting concrete
Deep learning
Artificial neural networks

ABSTRACT

The prediction of formwork pressure exerted by self-compacting concrete (SCC) remains a challenge not only to researchers but also to engineers and contractors on the construction site. This article aims to utilize shallow neural networks (SNN) and deep neural networks (DNN) using Long Short-Term Memory (LSTM) approach to develop a prediction model based on real-time data acquitted from controllable laboratory testing series. A test setup consisting of a two-meter-high column, ø160 mm, was prepared and tested in the laboratory. A digital pressure monitoring system was used to collect and transfer the data to the cloud on a real-time basis. The pressure was monitored during- and after casting, following the pressure build-up and reduction, respectively. The two main parameters affecting the form pressure, i.e., casting rate and slump flow, were varied to collect a wide range of input data for the analysis. The proposed model by DNN was able to accurately predict the pressure behavior based on the input data from the laboratory tests with high-performance indicators and multiple hidden layers. The results showed that the pressure is significantly affected by the casting rate, while the slump flow had rather lower impact. The proposed model can be a useful and reliable tool at the construction site to closely predict the pressure development and the effects of variations in casting rate and slump flow. The model provides the opportunity to increase safety and speeding up construction while avoiding costly and time-consuming effects of oversized formwork.

1. Introduction

Cast-in-place SCC is a common method in mass concreting where building or infrastructure elements are cast at the site in a preset formwork [1,2]. In such projects, SCC is preferred over the use of normal concrete because it offers high flowability, better working condition, and faster construction time [3]. One of the issues that is not fully resolved is the forecast of its lateral form pressure during and after pouring [4]. Designers still use the principle of hydrostatic pressure to design the form which is associated with high formwork cost and limits the casting rate [5]. Studies showed that SCC behaves differently in comparison with other liquid materials, and its properties change with time due to the agglomeration of particles and the viscosity behaviors when at rest it is high but when agitated it reduces [6]. Besides that, the hydration of cement, and the breakdown of its structure, it behaves as a liquid directly after mixing, but when the time passes it starts to be viscoelastic followed by its hardening due to the hydration of cement and the structural bonds created [7]. Therefore, designing the form using hydrostatic pressure may results in an over design leading to increased project costs. Furthermore, the speed of construction can be decreased thus outweighing part of the advantages of using SCC. Several studies showed that the actual form pressure exerted by SCC is lower than the hydrostatic pressure [2,8–42]. Hence, there is possibility to speed up the casting time while maintaining safe working place through well-established pressure prediction models.

The form pressure exerted by SCC is affected by various parameters related to mix design, materials characterization, fresh concrete properties, and placement methods [5,43,90]. The extent of the impact of these parameters varies significantly [5] and researchers tried to estimate these effects by considering certain specific parameters in the developed mathematical prediction models [8,9,43–46]. For instance, Ovarlez and Roussel [47] model was developed by using Janssen's (1885) silo theory and the model considered the time-dependent stress increase at rest, indicating thixotropic behavior. The model also considers form geometries i.e. height and thickness. The casting rate and fresh concrete density were also included in the model. Similarly, Beitzel

* Corresponding author.
E-mail address: yaser.gamil@ltu.se (Y. Gamil).

https://doi.org/10.1016/j.autcon.2023.104869
Received 17 June 2022; Received in revised form 4 April 2023; Accepted 11 April 2023
Available online 21 April 2023

[48] applied Janssen's silo theory, and the model considers the impact of structural build-up, casting rate, casting height, and form width dimension. Another model developed by Khayat & Omran [5] was created to account for the impact of casting depth, concrete temperature, casting rate, and the form's minimum lateral dimension. The time between consecutive casting layers, as well as the largest aggregate size. The German standard (DIN18218) [14], which has been revised and applied to determine the maximum lateral pressure, is the only known standard that models the pressure. To calculate the pressure, the model gives more concern for the setting time of concrete obtained using its own method defined in the standard, casting rate, and concrete unit weight as the impacting factors of pressure. In contrast, Gardner et al., [28] established a mathematical model based on several field measurements. The model considered the casting rate, and the time needed for the slump flow to decrease to zero. To summarize, there has been a significant research effort to develop a standard model for the design of formwork, while casting with SCC. However, the developed models have not been accepted as a design standard. To make use the time series data obtained through extensive laboratory experiments, more advanced methods can be applied to predict the pressure exerted by SCC. The objective of this research was to develop a method for predicting the form pressure using deep learning based on more inclusive time series data.

2. Applications of DNN in concrete technology

A deep neural network (DNN) is an artificial neural network (ANN) with multi-layers between the input and output layers it mostly consists of five components neurons, synapses, weights, biases, and functions [49]. DNN is part of machine learning which is based on an artificial neural network that gives the computer a learning ability from the data [50,51]. The way it works is by specified learning algorithms where the data are split into three non-equal data sets the largest used for training, while the other sets are for validation and testing [52]. DNN has been applied across different disciplines. In concrete technology, this method has been applied to predict parameters that are based on time series data for example fresh concrete properties [53] and hardened properties such as compressive strength [50,51,54–56].

To understand the extent of deep learning applications in concrete technology, a bibliometric analysis of the common research databases is performed using the VOS viewer tool. Three keywords are used as a search title which are deep learning in concrete, machine learning in concrete, and neural network in concrete in three databases' dimensions, web of science and Scopus from 2010 to 2022. Fig. 1 shows the network visualization of publications across different countries, it is shown that the most common research in machine learning is conducted in China followed by the United States. Above all, many other countries also do research related to machine learning, which proves the significant appreciation of deep learning, especially when studying time series

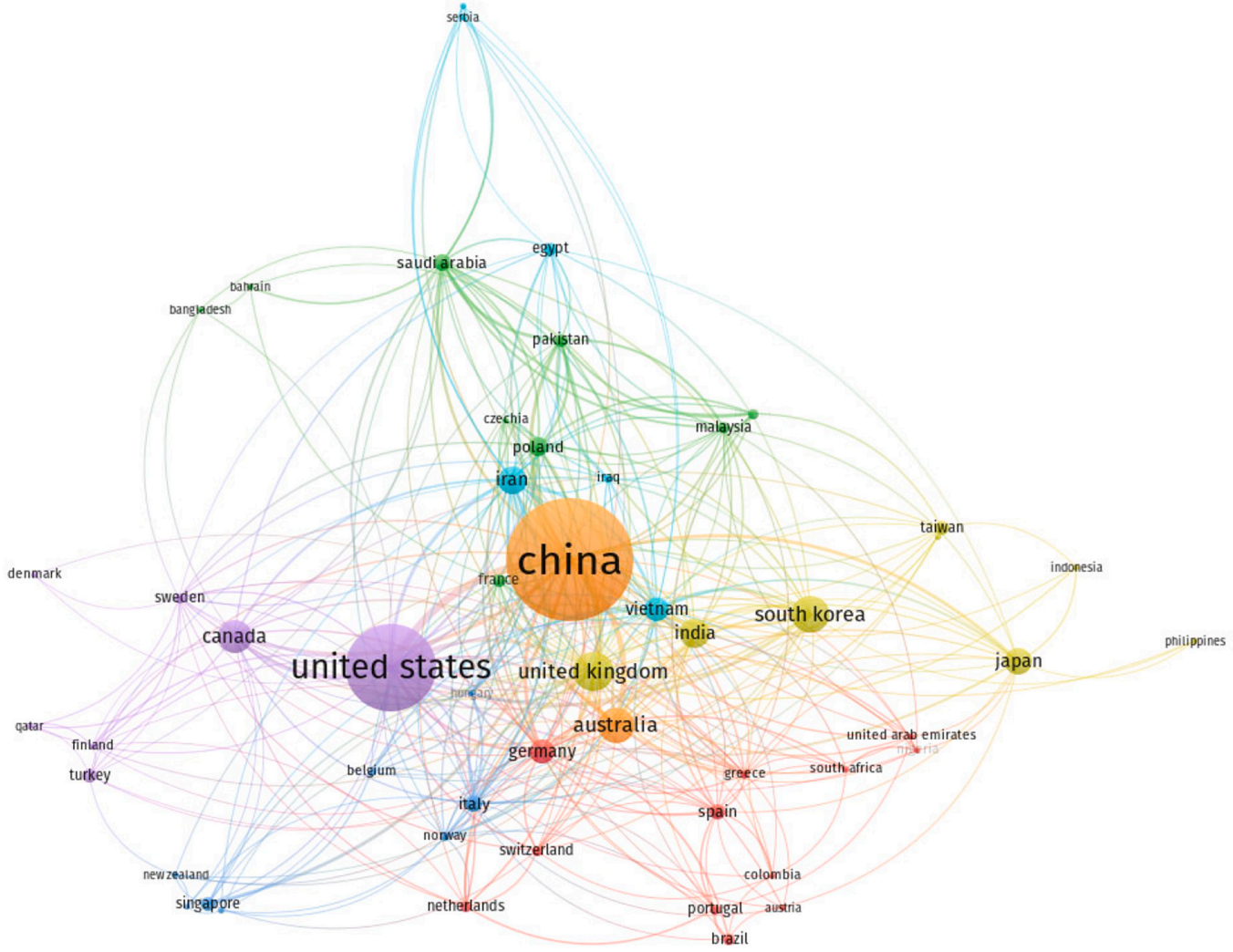

Fig. 1. Network visualization of publications across different countries.

datasets. Fig. 2 shows the visualization of publications based on keywords highlighted in the published articles and how deep learning is applied across different fields in concrete technology. While Fig. 3 shows the most dominant sources and journals focusing on deep learning in concrete technology.

DNN has been used in different areas, also including the prediction of properties during hardening and in the hardened state [56–60]. It is also used later for ready structures for the detection of cracks and surface defects, [52,61,62].

A study presented by [57] used DNN to predict the compressive strength of rubber concrete based on databases that incorporated data about the binder, aggregate, and other input parameters, while the output was the compressive strength. The results observed by the DNN model outperform in comparison with other neural network structures. Another study focused on the prediction of foamed concrete strength using DNN with high-order neurons [58] where the model was also developed using a dataset incorporating other machine learning methods. The sensitivity analysis was performed to evaluate the effects of input variables on the compressive strength and the model was deemed to be a reliable prediction tool for mixture design optimization of foamed concrete [58]. DNN was used to predict the compressive strength in recycled concrete [20,36,56,63–67]; the input parameters were water-cement ratio, recycled coarse aggregate replacement ratio, recycled fine aggregate replacement ratio, and fly ash replacement ratio, all of which were learned through convolutional neural networks; a set of 74 concrete blocks with various mix ratios were used to conduct the experiments; the developed model showed higher precision and efficiency [58].

The machine learning approach was also used to analyze the strength of a geopolymer concrete based on green fly ash [54]. The experimental work was performed on 335 mix proportions to produce the data for training and validating the model. The input parameters were the amount of fly ash, water glass solution, sodium hydroxide solution, coarse aggregate, fine aggregate, water, the concentration of sodium hydroxide solution, curing time, and curing temperature while the output parameter was the compressive strength- The model found to be accurate. DNN was also used to predict the flexural strength of concrete based on a data driven DNN [50]. The model used a Rectified Linear Unit function and a Sigmoid function as activation functions and a large perceptron's number, and the results showed an excellent accuracy of over 90% [50]. DNN was also used to estimate the mechanical properties of concrete containing silica fume exposed to high temperatures, the learning approach was stacked autoencoders and long short-term memory (LSTM) networks, [51].

The DNN was extended to be used in the operation time of construction projects as well. An analytical study tried to detect cracks in the concrete [59,68]. Handwriting scripts were used to develop a model based on a region convolutional neural network. The method can automatically allocate cracks based on the images [59]. Concrete flaws detection was also possible when Using Ultrasonic Tomography [69] and Convolutional Neural Networks. The DNN was also used to perform the structural design of reinforced concrete, where the prediction of wall dimensions was deemed to be adequate. The DNN was also used to find information between acoustic emission parameters and performance in concrete structures for structural health monitoring [70]. To conclude, many applications of DNN are valid and accurate and there is a possibility to employ this method to develop a prediction model for the pressure exerted by the cast-in-place SCC especially with the existence of advanced real-time data acquisition pressure systems.

3. Laboratory setup and data collection

The laboratory test included the preparation of formwork, mounting and installing the sensors, mix-proportioning, concrete casting, data sampling, and analysis of the data. A wireless digital pressure system was used to monitor the formwork pressure. The results were

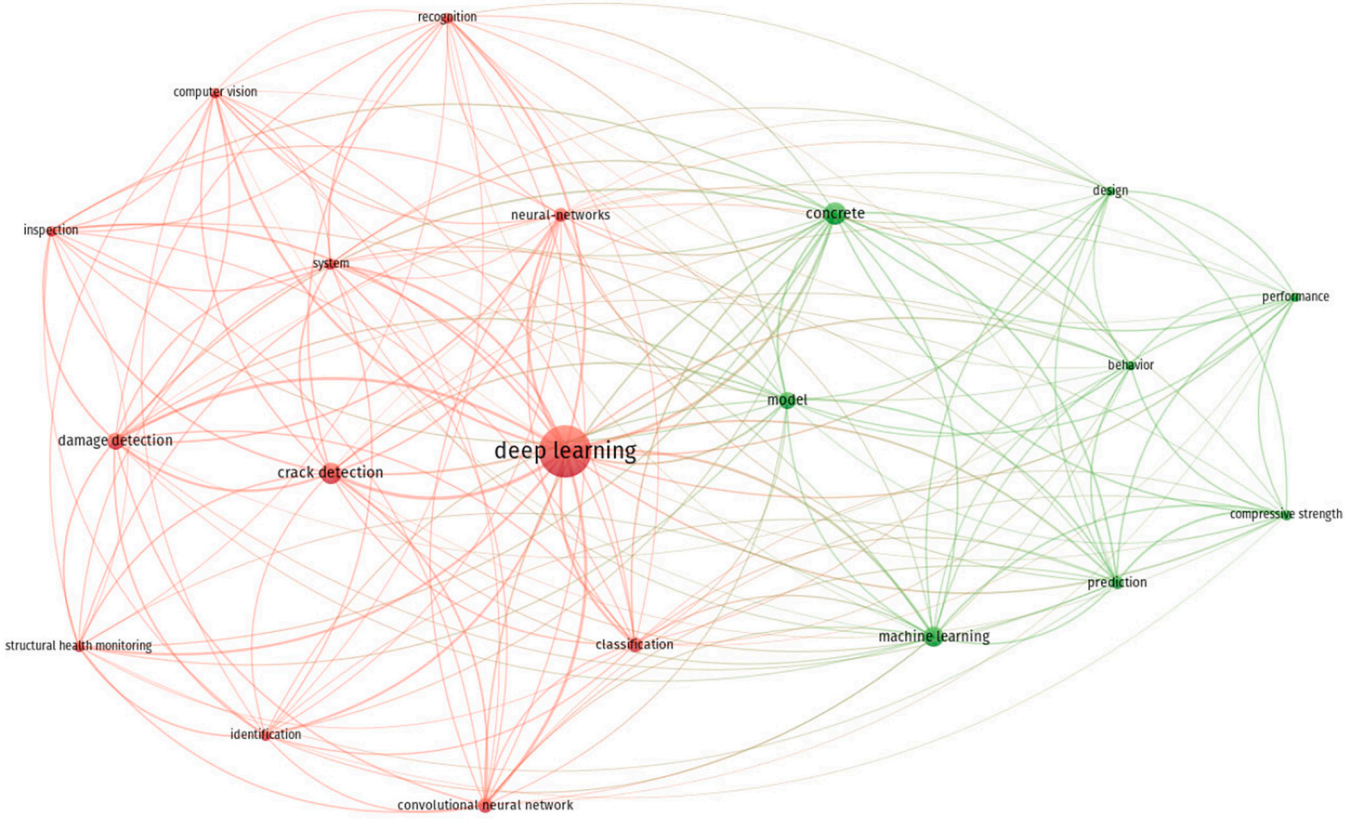

Fig. 2. Link between research publications based on keywords.

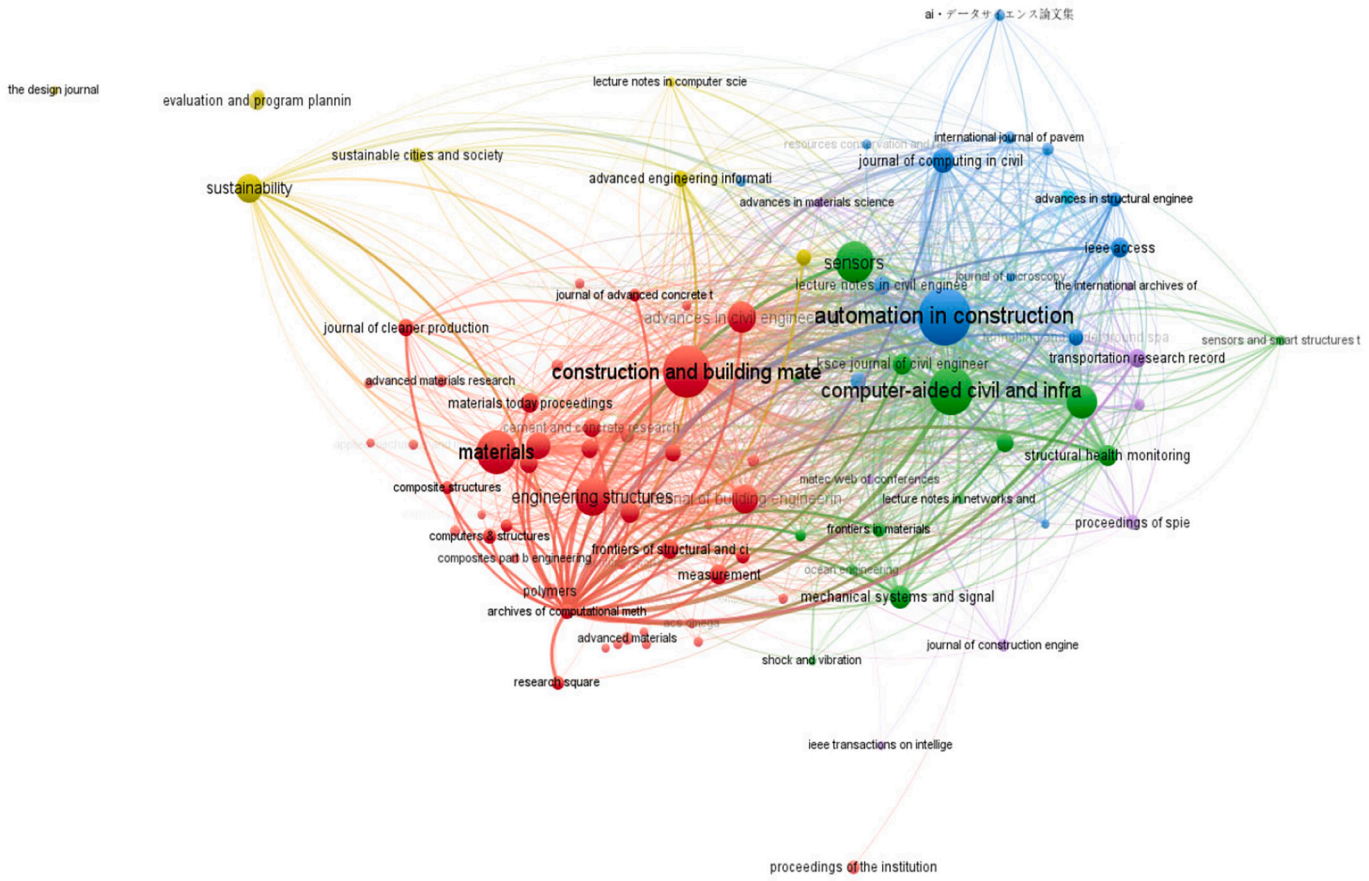

Fig. 3. Network visualization based on publications sources.

continuously transferred to the cloud, enabling a remote track of live data. The data then were collected and verified for all the tests and the model was created with MATLAB 2020b and Deep-Learning Toolbox (MathWorks), with the assistance of a computer with a single CPU and 4 gigabytes of memory. Fig. 4 shows a schematic explanation of the procedure and the methodology used to perform the laboratory tests.

The formwork within this study consisted of 2000 mm high, ø160 mm, circular columns. Transparent Polyethylene (PE) pipes were used to provide easy and precise visual information about the casting process and the filling rate. The pressure system consisted of four pressure sensors located 50 cm apart, the main transmitter unit, and an online database. The pressure system was developed by PERI. The system track data continuously to the cloud in one-minute intervals. Eight tests were performed in total, and the input parameters investigated were the casting rate and the initial slump flow. The pressure data was sampled for all tests and compiled for further refining and validation. The fresh concrete properties were tested for each concrete batch to maintain the variations of parameters. Mixing and placing of the concrete were performed in a controlled laboratory environment. A fresh mix was prepared for every casting.

4. Variation of parameters

The form pressure is affected by several material and physical properties, [43]. Three input parameters were investigated and varied in this study: the casting rate, and the initial slump flow, Table 1.

The same concrete recipe was maintained while changing only the amount of superplasticizer which is MasterGlenium 592. At first, the slump was maintained between 700 and 750 while changing the speed of casting and then the speed of casting was maintained, and the slump flow were varied to examine the different impact of these parameters on the form pressure. The water-to-cement ratio was maintained for all the mixes as 0.5, the reason is that maintaining the same water-to-cement ratio helps to limit the variation to change the slump flow by only adding Masterglenium which is the core of this laboratory plan. The cement type was CEM II/A-V 52.5 N Portland-fly ash cement manufactured to comply with requirements in SS-EN 197–1 Cement-Part 1. According to the supplier, Bascement is generally recommended to be used in standard concrete work, such as house construction.

5. Deep-learning algorithms for form pressure prediction

5.1. Data acquisition and processing

The data collected were in the form of time series, where reading was done in one-minute intervals during and after casting. It was obtained from four sensors and included pressure and time. The data were processed and validated to check for any outliers by comparing them with the hydrostatic pressure. The final datasets used for the development of the model originated from 8 columns cast in the laboratory. Firstly, the correlation between the input parameters was observed using all datasets. The input parameters were slump flow and casting rate while the output parameter was the lateral form pressure. The matrix shown in Fig. 5 indicates a strong correlation between the casting rate and the maximum form pressure. Thus, the casting rate had a stronger effect on the form pressure, which complied with other studies, [8,15,71]. The slump flow had minimal effect on the pressure. The diagonal for all is equal to 1 which indicates that each variable is perfectly correlated with itself.

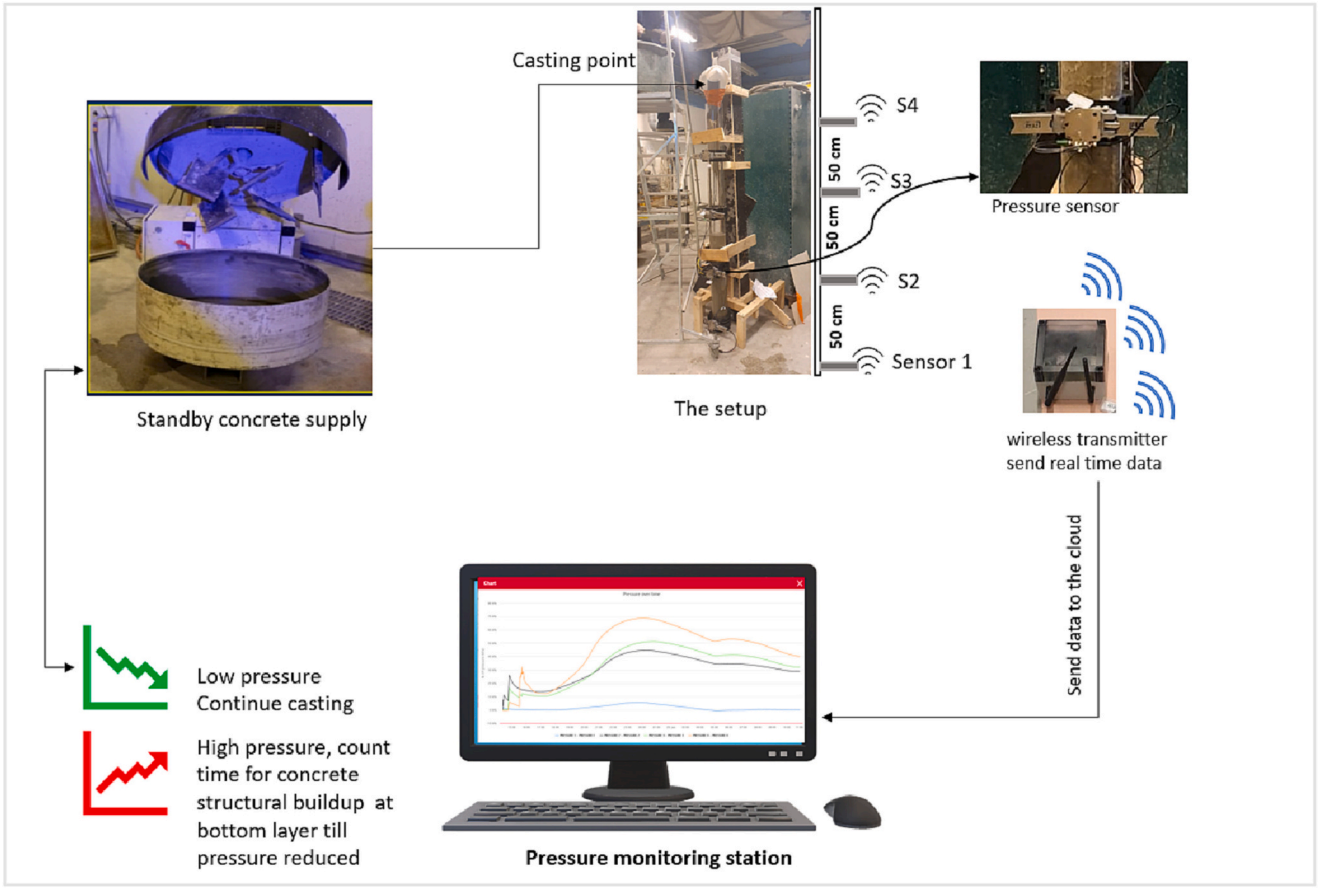

Fig. 4. Laboratory setup and digital pressure system.

Table 1
Variations of input parameters

Setup No	Casting rate (m/h)	Initial Slump flow (mm)
Setup 1	0.25	
Setup 2	0.5	700–750
Setup 3	1.0	
Setup 4	4	
Setup 5		600–700
Setup 6	0.5	500–600
Setup 7		400–500
Setup 8	0.5	700

5.2. Form pressure prediction using the shallow neural network

A shallow neural network (SNN) is a basic neural network that may be used for almost any purpose [72]. In this research, it was used as an estimation function model to predict the lateral pressure as a function of the slump flow and the casting rate value. The cement type and other parameters remained constant. In this section, a general overview of multilayer ANN will be given along with a focus on fitting the threshold criterion of the mode [73]. A perceptron is a fundamental building block of ANN, and the binary classifier was originally known as a perceptron. However, the perceptron is considered a function that takes certain inputs and outputs from the linear equation that is nothing more than a straight line. As shown in Fig. 6, this can be used to separate easily separable data.

A multilayer Perceptron is a fully connected neural network that has a Multiple Perceptron (MLP) [74]. For example, in Fig. 6, the MLP is designed with three layers in which one of them is hidden, then a deep ANN that has more than one hidden layer [52]. A feedforward ANN (FNN) such as the MLP, is a common example of an ANN, which shows that the connection between the nodes is not cyclic, which means there is no loop in the network, [75]. It is essential to propose the activation function, which shows the i^{th} activation unit in the l^{th} layer Fig. 7.

Three types of layers can be distinguished, the input layer a_i^{input} refers to the i^{th} value, and the i^{th} unit in the hidden layer is defined by a_i^{Hidden}. Finally, in the output layer, the i^{th} activation unit is referred to as a_i^{Out}. The weight coefficient from layer l to layer $l+1$ is represented by $w_{k,jl}$ network, and needs tuning. The input layer in the MLP is represented by the first vertical set of four neurons, Fig. 7. The next two vertical sets of neurons are part of the middle layer, which is also known as the hidden layer, and the final single neuron is part of the output layer. The neural network demonstrated above is one-layered. This is because the input layer is not typically considered a network layer. The input data is fed to a set of neurons, each of which produces an output. Each of these outputs is again fed to other neurons, which produces another output, and then fed to the output layer. The error calculated at this output layer is sent back into the network to refine the outputs of each neuron, which are then fed to the neuron in the output layer to produce a more refined output than before.

While using a closed loop of back and forward propagation cycles, the MLP learning procedure is repeated until an output with a minimal error is obtained [76]. The number of layers and neurons is referred to as neural hyperparameters. The entire learning phase can be divided into five steps, i.e., 1) learning starts with the input layer and progresses to the output layer and this is known as forward propagation, 2) calculating the error based on the output (the difference between the predicted and known outcome whereas the error must be kept to a minimum, 3) propagate the error in the back direction and find its derivative concerning each network weight and update the model, 4) learn ideal weights, repeat the three steps over multiple epochs, and 5) finally,

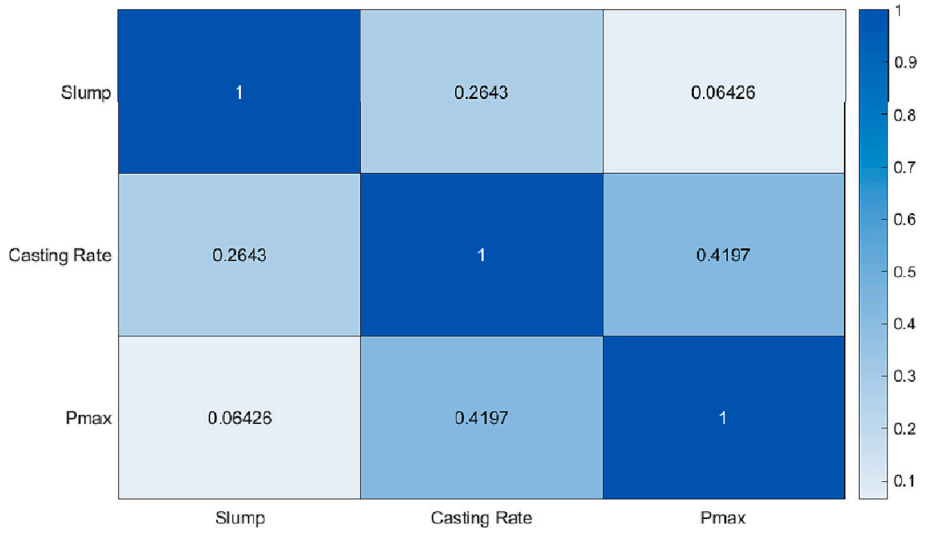

Fig. 5. Correlation matrix between input and output parameters.

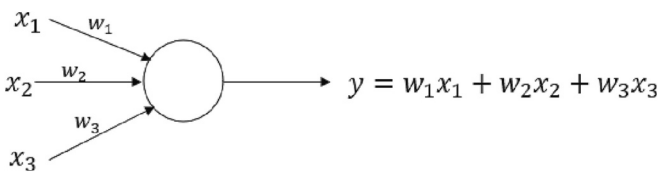

Fig. 6. A perceptron model for constructing the ANN.

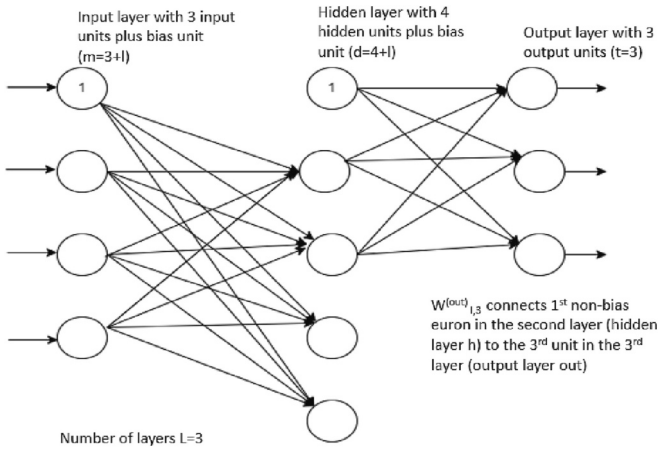

Fig. 7. Activation function.

the predicted value is obtained by passing the output through a threshold function, [77]. The first and third steps are the most important components of the MLP network. In the MLP, the first step is known as Forward Propagation (FP). The eqs. (1) and (2) were used to calculate the activation unit al(h) in the hidden layer:

$$Z_1^{(h)} = a_0^{(in)} w_{0,1}^{(h)} + a_1^{(in)} w_{1,1}^{(h)} + \ldots + a_m^{(in)} w_{m,1}^{(h)} \quad (1)$$

$$a_{01}^{(h)} = \varnothing\left(Z_1^{(h)}\right) \quad (2)$$

The activation function φ is often the sigmoid (logistic) function. It enables the nonlinearity required to solve complex problems such as image processing [78]. Following the generation of the output, the error (or loss) is calculated, and a correction is sent back through the network. This is known as 'back propagation' (Step 3). There are several methods for implementing this step; however, in this research, the Stochastic Gradient Descent (SGD) was used as an algorithm [79]. To reach the minimal point, the SGD algorithm continuously updates the initialized weights in the negative direction of the slope [80]. In this approach, the goal is to create a model that can predict the maximum pressure for any predefined combination of casting rate and slump flow after time. All data were gathered in a random order in one list, for an appropriate combination of inputs and outputs for each time interval. Fig. 8 presents 50% of data originating from all 8 setups. In each setup 480 values of the maximum pressure were measured for the first 8 h after casting and for every 60 s. Fig. 8 shows the data used for the learning phase, which were obtained from the actual laboratory measurements.

Before starting the modulation using the MLP a basic visualization process was made to check if the data is uniformly distributed before feeding into the model. The maximum measured pressure was uniformly distributed and varied between 0 and 40, Fig. 9.

A simple shallow ANN architecture with three inputs was used in the first layer. At first, the model was fed with the slump, casting rate values, and time stamps from the sensor for each reading. The model only had one hidden layer and one output, which was the predicted maximum pressure. The number of neurons for each hidden layer was tuned as a parameter. The number of neurons for each hidden layer was tuned as a hyperparameter. These neurons in the hidden layer generated new features that combined the original inputs to predict the maximum pressure as an output for the ANN model. The dataset was divided into 3 fractions, i.e., 50%, 30%, and 20%. Whereby 50% of the data was used for the model development, and 30% was used to validate the model. 20% of the data was used for testing the model. The training set was used to extract the needed features, validate the set used to optimize and tune the number of neurons in the hidden layer, and finally test the set to see how well the model will perform when using a completely new set of data. The first step is feeding with the training data, over multiple epochs, to update the values for the ANN weights. The forward propagation and then optimization of these connections between all neurons using the SGD backpropagation process was done. Several other possible hyperparameters could be optimized, i.e., the type of the activation function, the learning rate, or the type of the learning method. However, these parameters have less effect on the accuracy of the model, and they are selected randomly as default parameters, Table 2. These parameters are used for optimization purposes [81].

As described before, the test dataset was used to foresee how well the model is predicting the maximum pressure using data that the model has never seen during the training and validation phases.

The MLP consists of an input layer with all the input attributes and an

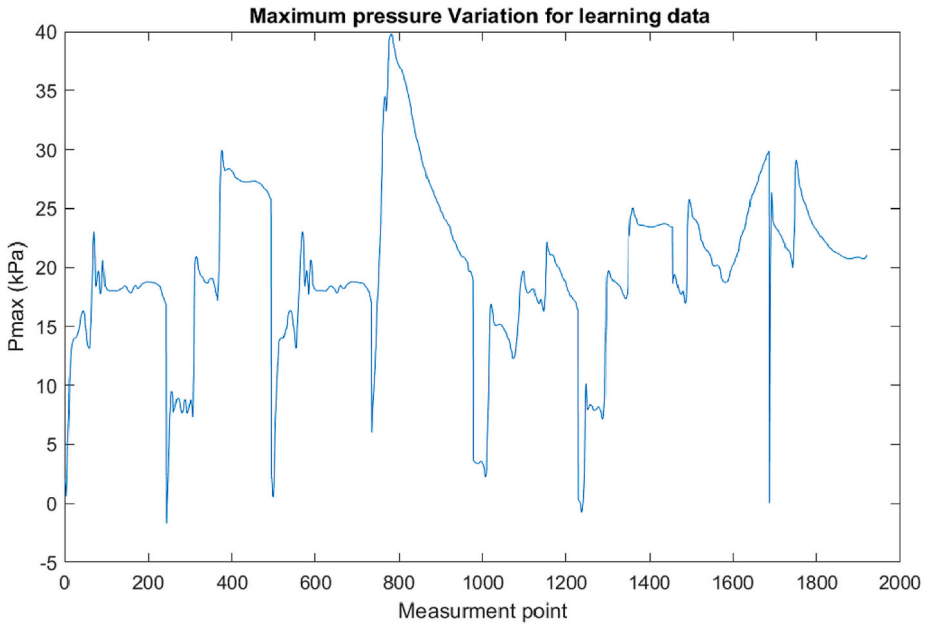

Fig. 8. Maximum pressure variations for learning data.

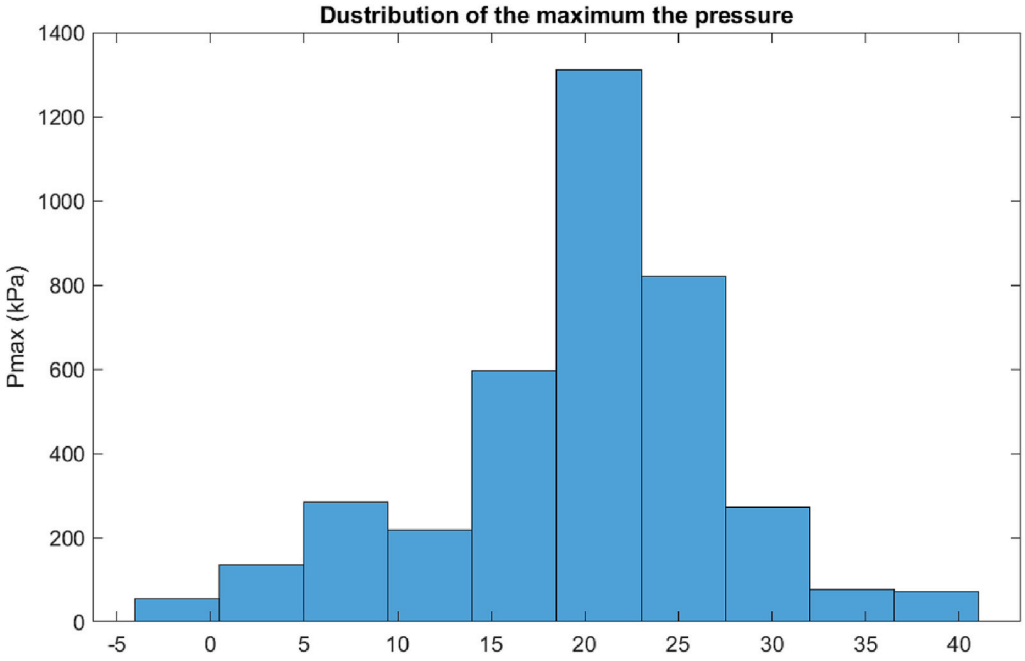

Fig. 9. Data visualization for uniformity check, distribution of Pmax.

Table 2
default model parameters.

Hyperparameter	Value/approach
Activation function	Tan-Sigmoid
Learning method	Levenberg-Marquardt backpropagation
Number of iterations	54
Number of epochs	1000
Batch size	35
Performance measure	Mean Square Error (MSE)
Learning rate	0,05

output layer with just 1 neuron that represents the predicted maximum pressure. In this study, several architectures of ANN with a different number of neurons in the hidden layer have been tested. The number of neurons in the input layer and the output layer was determined by the number of input variables and the number of targets planned to be predicted. A small routine was used to compare the effect of the number of neurons on the accuracy of the prediction with different architectures that used 1 to 70 neurons in the hidden layer. In Fig. 10 the blue curve presents the Root Mean Square error (RMSE) for different numbers of neurons in the training phase. The RMSE error was calculated using the formula below:

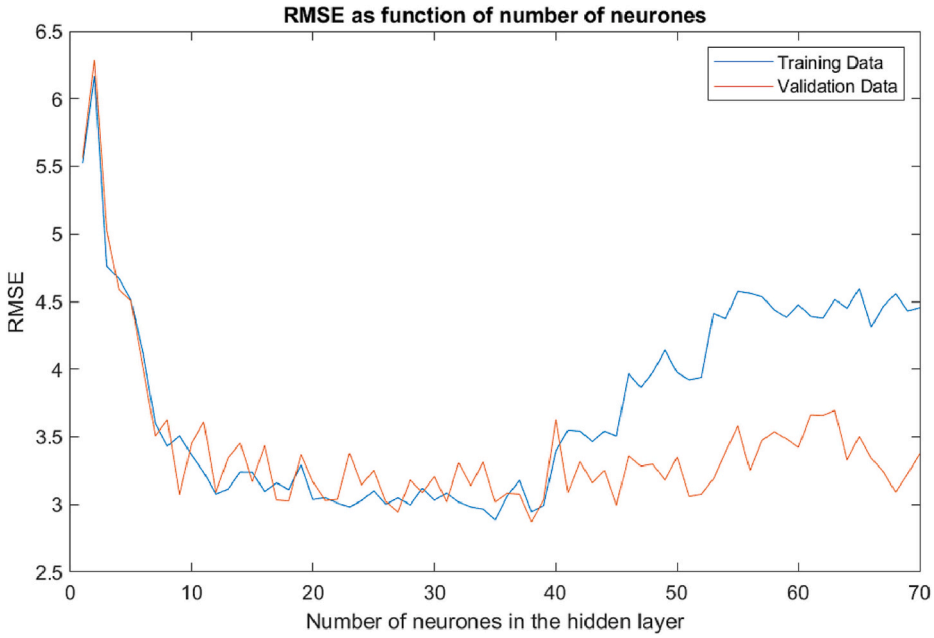

Fig. 10. RMSE as a function of the number of neurons.

$$RMSE = \sqrt{\frac{\sum_1^N \left(Pmax_i^{Predicted} - Pmax_i^{Actual}\right)^2}{N}} \quad (3)$$

The performance of the model is measured in terms of Root Mean Square error (3). The output of the real maximum pressure value was used and the MLP model output as a predicted value for 7 independent setups to validate the proposed model based on the RMSE performance metric. (Table 3).

In Fig. 10, the orange curve and the blue curve are the same presentations for the RMSE value but a different choice of neurons in the hidden layer, respectively for the learning data and the validation data. Typical underfitting and overfitting behaviors for the MLP model could be seen. When the number of neurons was low the model was under fitted and both RMSE errors for the training and validation phase were quite high. It could be related to the usage of a very simple and which has a high bias that fits only partially the data. It was impossible to interpolate the existing relationship between the casting rate, the slump flow, and the maximum pressure. On the other hand, if the number of neurons was too high, the complexity of the model would increase which will result in lower accuracy of the prediction in the validation phase. The model was overfitted and had a high variance. It fitted only the learning data and generalization of the relationship was impossible. The best accuracy for the shallow MLP neural network was achieved when 38 neurons were present in the hidden layer, Fig. 10. It provided the best MLP architecture with the lowest RMSE and the best fit that generalized the overall behavior of the data Fig. 10. The final accuracy of the MLP shallow neuron network model for the training and testing data was respectively 2.92% and 2.94%, Fig. 11.

Table 3
independent steps for model validation.

Number of hidden Neurons	RMSE Training data	RMSE Validation data
10	3.63	3.47
20	3.03	3.16
30	3.03	3.2
40	3.39	3.62
50	3.34	3.13
60	3.42	4.47
70	3.37	4.45

5.3. Form pressure prediction using LSTM

The second used model, the ANNs, is part of the machine learning family. An LSTM network is a Recurrent Neural Network (RNN) that processes input data by iterating over time steps and updating the network state [82]. The network state contains information remembered over all previous time steps. The LSTM network was used to forecast the next pressure reading based on the previous reading as input [83,84]. The LSTM is a subcategory of RNN that addresses the hidden gradient problem, considers time, and solves the problem of storing short-term data over long periods [82]. The LSTM architecture is highly recommended for the temporal modeling of sequence data [85]. The key idea behind the LSTM theory is a memory block that remembers its state during the training process [86]. It is possible to keep old features acquired at the start of the training phase and new features acquired by the end of the training with the memory block [83]. The LSTM process expressed mathematically is presented in eqs. 4 to 9.

$$c_t = f_t \otimes c_{t-1} + i_t \otimes \tilde{c_t} \quad (4)$$

$$h_t = o_t \otimes tanh(c_t) \quad (5)$$

$$\text{Where } f_t = \sigma\left(W_{fh}h^{t-1} + W_{fx}x^t + b_f\right) \quad (6)$$

$$i_t = \sigma\left(W_{ih}h^{t-1} + W_{ix}x^t + b_i\right) \quad (7)$$

$$c_t = tanh\left(W_{ch}h^{t-1} + W_{cx}x^t + b_c\right) \quad (8)$$

$$o_t = \sigma\left(W_{oh}h^{t-1} + W_{ox}x^t + b_o\right) \quad (9)$$

The weights for the forget gate, input gate, input modulation, and output gate are $W_{f\ h}$, $W_{f\ x}$, W_{ih}, W_{ix}, W_{ch}, W_{cx}, W_{oh}, and W_{ox}, respectively. Immediately preceding propagation provided three inputs to the cell. The input is processed using internal gates tanh which are governed by the hyperbolic tangent function and the sigmoid function, respectively. The bases matrices are b_f, b_i, b_o, and b_c, and they are not time-dependent, which means they do not update from one time step to the next.

Fig. 12 illustrates the input and output flow of an LSTM for one timestep. This is a single timestep input, with output governed by Eqs. (4) and (5). Each LSTM cell has an input xt, ht-1, and ct-1, which are the

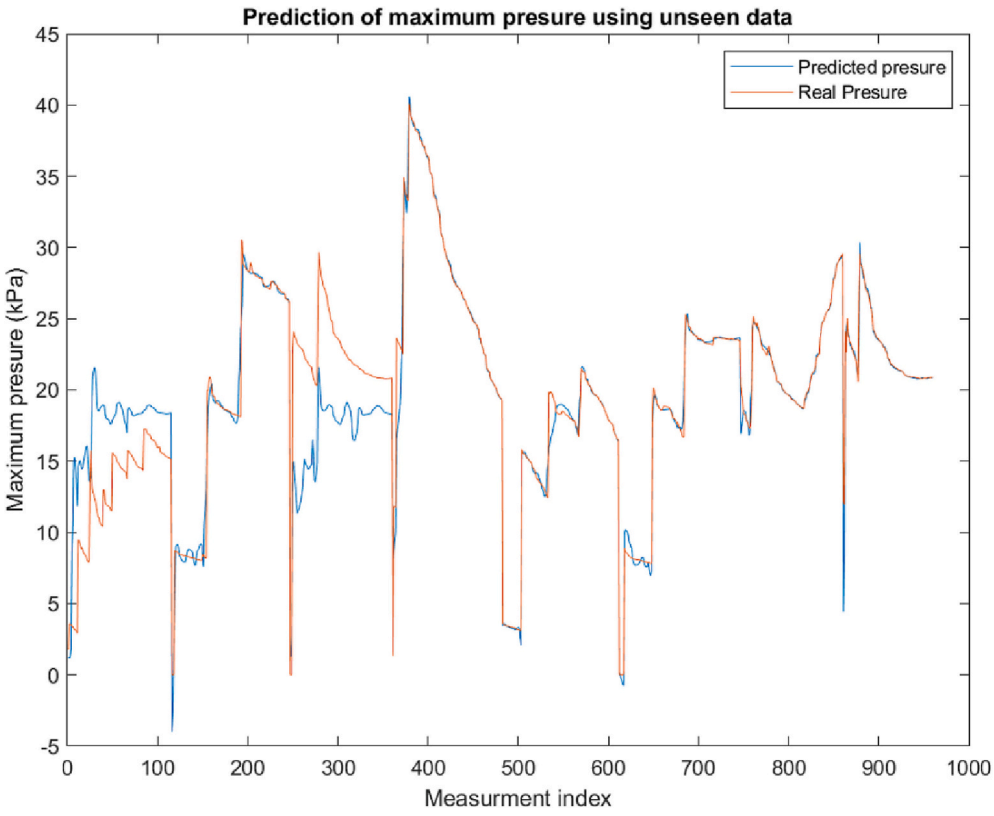

Fig. 11. Maximum pressure prediction using MLP.

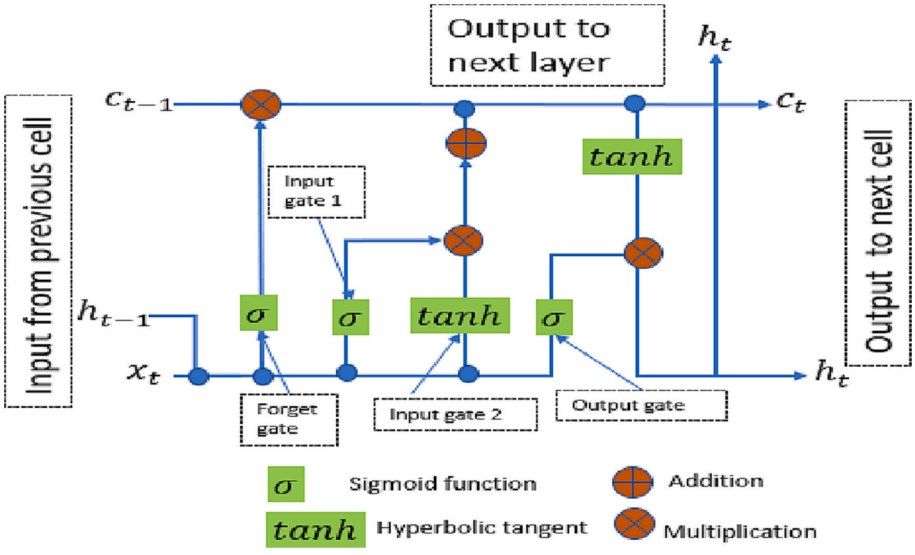

Fig. 12. Input and output flow of LSTM for one timestep redrawn from [81].

inputs from the previous timestep LSTM. o_t show the output of the LSTM cell for the current timestep. The LSTM also generates the ct and ht. for feeding the next time step LSTM. The internal gates will determine the amount of information that can be updated into the hidden state h and the cell state c based on the current input x, the internal state c, and the hidden state h. This behavior allows the LSTM cell to discover new patterns and features.

In this research, the data was treated as a time series input for the ANN model. In contrast to the previous model, only the pressure variable was used as model input. Another distinction was that the data were not compiled into a single list, but rather each setup containing 480 pressure reading values was handled separately. The goal was to forecast time series data using a long short-term memory (LSTM) network. Six setups obtained from the experiments were used to build the model, with two additional setups serving as test data. (Fig. 13).

In the proposed approach, the regression of the LSTM network was trained where the target was the training sequences with pressure reading shifted by one-minute step. In other words, at each minute, the LSTM network learns to predict the maximum pressure of the next minute. A recurrent neural network (RNN) that processes the input data

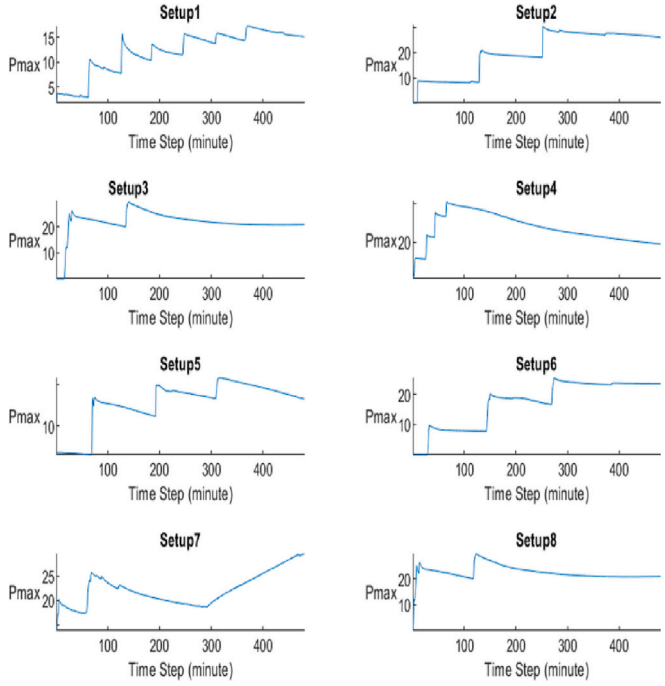

Fig. 13. Actual maximum pressure vs time obtained from the experimental monitoring.

by looping over time steps and updating the network state was the LSTM network. The network state stored information from all previous time steps. Hence the LSTM network predicted the next pressure reading based on the previous reading as input.

Pressure forecasting can be done in two ways: open loop and closed loop. To suit the nature of the data collected in this research, an open loop was used. Based on the past data, the open loop forecasting predicted the next time step in a sequence. When making predictions for time series data, the actual past data were used as input. Most of the literature suggests that machine learning algorithms use cross-validation. This, however, is not a general assumption. In his book, Shalev-Shwartz [87] confirms that it is sometimes better not to use cross-validation. Overfitting is one disadvantage of using cross-validation. Essentially, cross-validation techniques are used to tune the model parameters on the validation data set but not on the test data set. However, once the model has been tested, this fine-tuning can occasionally go too far, resulting in a lack of generalization. Furthermore, cross-validation is more necessary because there was not enough training data, and it is unsure that the model is generalizable further than the sample data used during the training phase. In this case, because a research test rig is used, the advantage is to generate as much data as the need and have complete control over the scenarios, then more attempt is advised when collecting data.

All previous readings from time steps 1 through t1 were used to predict the maximum pressure for the next time step t. After that, a new sensor reading was waited for time step t and used as an input to make the next prediction for time step t + 1. To prevent the training from diverging, the predictors and targets were normalized to have zero mean values and unit variance. The test data were also normalized using the same metrics as the training data when making predictions. The normalized pressure was calculated based on the mean (μ) and standard deviation (σ) as shown in eq. (10):

$$Pmax_{normalized} = \frac{P_{max} - \mu}{\sigma} \tag{10}$$

The following step was to define the network architecture to build the LSTM regression network. Because there was only one target to predict, a sequence input layer with one neuron was used in the input layer. It was decided to use an LSTM layer with 128 hidden units. The layer's learning capacity was determined by the number of hidden units. Using more hidden units could have produced more accurate results, but it could lead to overfitting of the training data. A fully connected layer with an output size that matches the input data was used. Finally, the regression layer was included as well. A fully connected layer with an output size that corresponds to the input data was used and a regression layer to the final network was added.

Some setting parameters in an LSTM model, such as the number of epochs and the initial learning rate, are very important for training performance [88]. A specific task for hyperparameter optimization is not used in this paper. However, the main hyperparameters, such as the number of training epochs and training batch size, are only tuned to interpret the results' accuracy. A simple comparison shows that the choice of setting the number of epochs and the size of training batches respectively to 80 and 35 is better than the tested alternatives.

There are several training options and hyperparameters that could be adopted. In this case, Adam optimization was used to train the model [89]. Since the data were limited to 100 epochs were used to achieve good accuracy. The learning rate was fixed at 0.001. In this approach, the first step was to split the data, allocating 80% of the data for learning and 20% for testing. The training data contained 4 sequences for different setups of a fixed length equal to 480. The model took about 73 s to learn and about 4 s to infer using a sequence of pressure data. The formulation shown in eq. (11) was used to assess the model's performance.

$$Accuracy = \frac{\sum(Level_{pred} == Level_{test})}{Number\ \ of\ \ test\ \ sequences} \tag{11}$$

The goal of the proposed open-loop prediction approach was to predict the next maximum pressure during the casting process. In this case, one minute was used as a time step as proof of concept, but it could be hours or any interval relevant to the total casting time. When making predictions for subsequent time steps, the true pressure reading was collected from the sensor for a while, and then these data were used as input to predict what will be the maximum pressure in the next time step. To do so, the model had to be initialized using the first readings from the sensors. For further predictions, the model needs to be updated with the actual previous readings. In this care, the first 40 readings were reserved for the initialization, and the prediction began after 41 min. Based on the output of the real maximum pressure value and the LSTM model output as a predicted value, a validation is performed for the proposed model using the Accuracy performance metric for different setups. (Table 4).

As shown in Figs. 14 and 15, the obtained LSTM model provided satisfactory results with an average accuracy for the learning data of 92,06%. The average prediction accuracy using the test data collected from setup 7 and setup 8 is 94.48% and 88.72% respectively.

The predicted maximum pressure by LSTM followed the trend of the actual maximum pressure measured in the laboratory. This indicates the model is accurate and achieved high accuracy. The model deems to be reliable for pressure prediction while casting with self-compacting concrete considering the casting rate and slump flow as the main

Table 4
accuracy performance indicators.

# Setup	Accuracy (%)
1	96.82
2	90.34
3	86.55
4	93.60
5	91.63
6	88.73
7	94.48
8	88.72

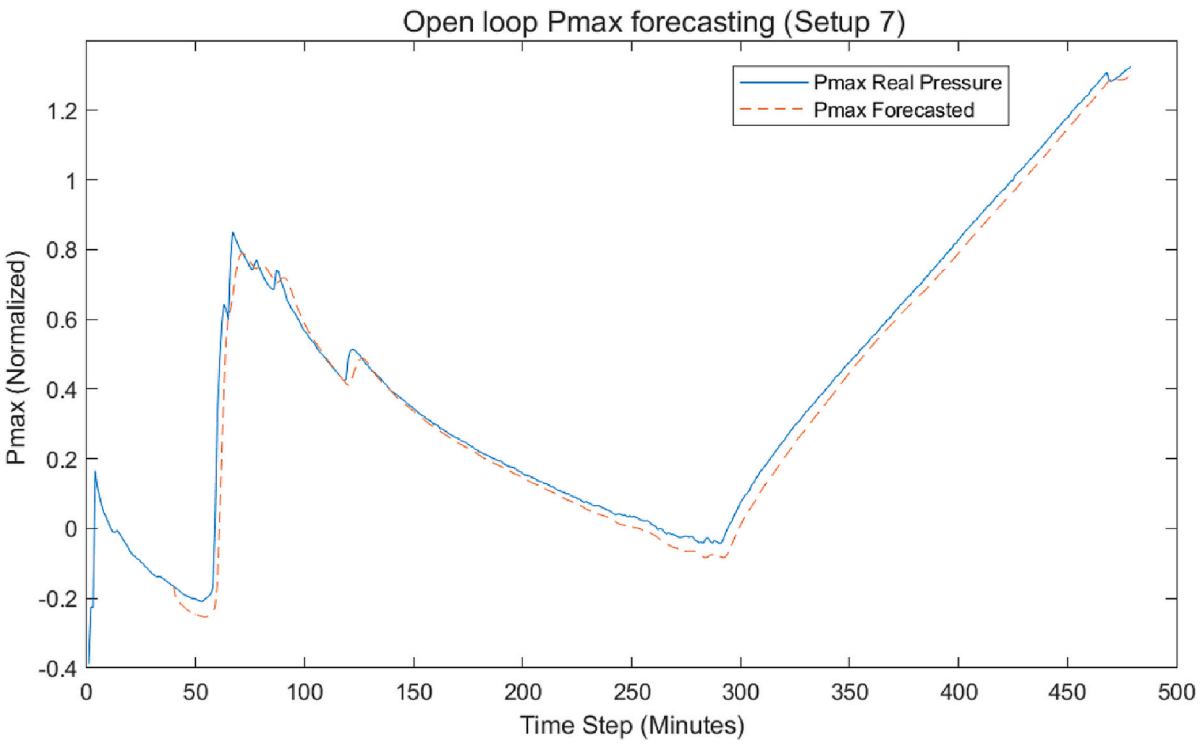

Fig. 14. Open-loop maximum pressure forecasting (setup 7).

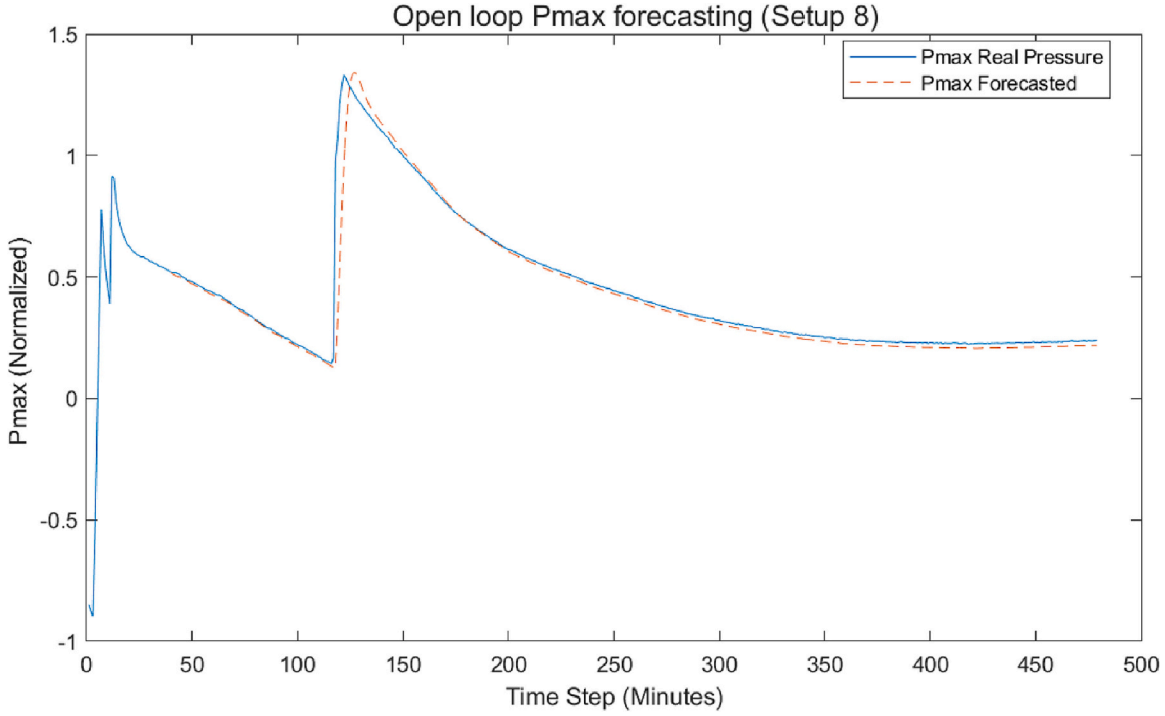

Fig. 15. Open-loop maximum pressure forecasting (setup 8).

input parameters.

6. Conclusions

In this article, deep learning applications based on SNN, and LSTM were used to analyze and predict the formwork pressure for cast-in-place self-compacting concrete. The actual data within this analysis were sampled from eight ø160 mm, 2000 mm high, circular columns, cast in the MCE laboratory at Lulea University of Technology, Sweden. Real-time data was continuously collected during and after the casting process, using a newly developed wireless, digital pressure system.

It is concluded that SNN can accurately predict the form pressure based on the historical input data. The results showed that the differences between the tested pressures and the SNN-model predictions were

relatively small. Similar results, with high prediction accuracies, were seen in all tests, even with variations in the input parameters in terms of casting rate and slump flow. The SNN model could potentially be used to accurately predict the form pressure in real-time basis on the construction site. This would allow engineers to make safe and reliable predictions, as well as adjust the casting rates, based on planned or unplanned variations in concrete properties and -deliveries.

The second model was developed using LSTM, which is a machine learning tool, using RNNs to process the input data from the laboratory tests, iterating the pressure history over time steps, and using the information to predict pressure development. The LSTM model showed satisfactory results with an average accuracy of 92,06% for the tests within this study. The results of this study indicate that deep learning solutions offer great potential in terms of accurately estimating the formwork pressure based on historical data. The findings presented in this paper could potentially help concrete constructors to estimate the pressure development based on the actual properties of the concrete delivered to the construction site, allowing them to make accurate decisions to cast faster and safer. Further studies are however needed to address other affecting parameters whilst utilizing the machine learning solution.

Funding

This research was funded by the Development Fund of the Swedish Construction Industry (SBUF) and NCC construction company.

Declaration of Competing Interest

The authors declare that they have no known competing financial interests or personal relationships that could have appeared to influence the work reported in this paper.

Data availability

No data was used for the research described in the article.

References

[1] S. Li, S. Yin, W. Yang, Research on the bonding performance of TRC permanent formwork and cast-in-place concrete, Eng. Struct. 235 (2021), 112021, https://doi.org/10.1016/j.engstruct.2021.112021.
[2] M. Arslan, O. Şimşek, S. Subaşı, Effects of formwork surface materials on concrete lateral pressure, Constr. Build. Mater. 19 (4) (2005) 319–325, https://doi.org/10.1016/j.conbuildmat.2004.07.007.
[3] M.K. Hurd, Lateral pressures for formwork design, Concr. Int. 29 (6) (2007) 31–33. https://www.concrete.org/publications/internationalconcreteabstractsportal.aspx?m=details&id=18662.
[4] P. Billberg, Form Pressure Generated by Self-Compacting Concrete: Influence of Thixotropy and Structural Behaviour at Rest. School of Architecture and the Built Environment Division of Concrete Structures, Royal Institute of Technology, Sweden, 2006. http://www.diva-portal.org/smash/get/diva2:10913/fulltext01.pdfThe.
[5] Khayat and Omran, *State-of-the-Art Review of Form Pressure Exerted by Self-Consolidating Concrete*, in *Ready-Mix Concrete Research Foundation*, Université de Sherbrooke, Canada, 2009. https://www.researchgate.net/publication/238723384.
[6] Y. Vanhove, C. Djelal, Formwork pressures with self-compacting concrete, Concrete-London-Concrete Soc. 36 (6) (2002) 22–23. https://www.researchgate.net/publication/259289532_Formwork_Pressures_with_Self-Compacting_Concrete.
[7] K.H. Khayat, G.D. Schutter, Mechanical Properties of Self-Compacting Concrete Vol. 14, Springer, 2014, https://doi.org/10.14359/12460.
[8] S. Teixeira, A. Santilli, I. Puente, Analysis of casting rate for the validation of models developed to predict the maximum lateral pressure exerted by self-compacting concrete on vertical formwork, J. Build. Eng. 6 (2016) 215–224, https://doi.org/10.1016/j.jobe.2016.03.008.
[9] Emanuelsson, Calculation Models for Calculating Lateral Pressures on Formwork when Using Self-Compacting Concrete, Luleå Tekniska Universitet, Luleå, Sweden, 2018.
[10] Omran, K. Khayat, Choice of thixotropic index to evaluate formwork pressure characteristics of self-consolidating concrete, Cem. Concr. Res. 63 (2014) 89–97, https://doi.org/10.1016/j.cemconres.2014.05.005.
[11] R. McCarthy, J. Silfwerbrand, Comparison of three methods to measure formwork pressure when using SCC, Concr. Int. 33 (6) (2011) 27–32. http://kth.diva-portal.org/smash/record.jsf?pid=diva2%3A485679&dswid=-6004.
[12] K. Assaad, Correlating thixotropy of self-consolidating concrete to stability, formwork pressure, and multilayer casting, J. Mater. Civ. Eng. 28 (10) (2016) 04016107, https://doi.org/10.1061/(ASCE)MT.1943-5533.0001624.
[13] S.H. Kwon, J.H. Kim, S.P. Shah, Development and applications of the intrinsic model for formwork pressure of self-consolidating concrete, Int. J. Concrete Struct. Mater. 6 (1) (2012) 31–40, https://doi.org/10.1007/s40069-012-0003-2.
[14] DIN18218, DIN standard on formwork pressures updated, Concr. Int. 1 (2010) 27–29. DOI: https://www.concrete.org/publications/internationalconcreteabstractsportal/m/details/id/51663776. DOI:.
[15] Assaad and Khayat, Effect of casting rate and concrete temperature on formwork pressure of self-consolidating concrete, Mater. Struct. 39 (3) (2006) 333–341, https://doi.org/10.1007/s11527-005-9042-3.
[16] Omran and Khayat, Effect of formwork characteristics on SCC lateral pressure, J. Mater. Civ. Eng. 29 (5) (2017) 04016293, https://doi.org/10.1061/(ASCE)MT.1943-5533.0001827.
[17] J.H. Kim, M. Beacraft, S.P. Shah, Effect of mineral admixtures on formwork pressure of self-consolidating concrete, Cem. Concr. Compos. 32 (9) (2010) 665–671, https://doi.org/10.1016/j.cemconcomp.2010.07.018.
[18] J.H. Kim, N. Noemi, S.P. Shah, Effect of powder materials on the rheology and formwork pressure of self-consolidating concrete, Cem. Concr. Compos. 34 (6) (2012) 746–753, https://doi.org/10.1016/j.cemconcomp.2012.02.016.
[19] Khayat Omran, Elaguab., Effect of SCC mixture composition on thixotropy and formwork pressure, J. Mater. Civ. Eng. 24 (7) (2012) 876–888, https://doi.org/10.1061/(ASCE)MT.1943-5533.0000463.
[20] P. Matar, Assaad., Effect of vertical reinforcing bars on formwork pressure of SCC containing recycled aggregates, J. Build. Eng. 13 (2017) 159–168, https://doi.org/10.1016/j.jobe.2017.08.003.
[21] Assaad and Khayat, Effect of viscosity-enhancing admixtures on formwork pressure and thixotropy of self-consolidating concrete, ACI Mater. J. 103 (4) (2006) 280, https://doi.org/10.14359/16612.
[22] Khayat and Assaad, Effect of w/cm and high-range water-reducing admixture on formwork pressure and thixotropy of self-consolidating concrete, ACI Mater. J. 103 (3) (2006) 186, https://doi.org/10.14359/15852.
[23] S.H. Kwon, Q.T. Phung, H.Y. Park, J.H. Kim, S.P. Shah, Effect of wall friction on variation of formwork pressure over time in self-consolidating concrete, Cem. Concr. Res. 41 (1) (2011) 90–101, https://doi.org/10.1016/j.cemconres.2010.09.009.
[24] Khayat and Omran, A, Evaluation of SCC formwork pressure, Concr. Int. 32 (6) (2010) 30–34. DOI: https://www.concrete.org/publications/internationalconcreteabstractsportal/m/details/id/51663748. DOI:.
[25] N.S. Saleem, M.H. Baluch, M.K. Rahman, M. Al-Osta, Experimental investigations and a new numerical model for evolution of formwork pressure in SCC, Arab. J. Sci. Eng. 42 (9) (2017) 3907–3921, https://doi.org/10.1007/s13369-017-2509-z.
[26] A. Gregori, R.P. Ferron, Z. Sun, S.P. Shah, Experimental simulation of self-consolidating concrete formwork pressure, ACI Mater. J. 105 (1) (2008) 97, https://doi.org/10.14359/19212.
[27] S.H. Kwon, Q.T. Phung, H.Y. Park, J.H. Kim, S.P. Shah, Experimental study on effect of wall friction on formwork pressure of self-consolidating concrete, in: 6th International RILEM Symposium on Self-Compacting Concrete and 4th North American Conference on the Design and Use of SCC, SCC, 2010. https://www.researchgate.net/publication/255720982_Experimental_study_on_effect_of_wall_friction_on_formwork_pressure_of_self-consolidating_concrete.
[28] N.J. Gardner, L. Keller, R. Quattrociocchi, G. Charitou, Field investigation of formwork pressures using self-consolidating concrete, Concr. Int. 34 (1) (2012), https://doi.org/10.1016/j.cemconcomp.2014.02.003.
[29] N.J. Gardner, L. Keller, R. Quattrociocchi, G. Charitou, Field investigation of formwork pressures using self-consolidating concrete, Concr. Int. 34 (1) (2012), https://doi.org/10.1016/j.cemconcomp.2014.02.003.
[30] T. Proske, K.H. Khayat, A. Omran, O. Leitzbach, Form pressure generated by fresh concrete: a review about practice in formwork design, Mater. Struct. 47 (7) (2014) 1099–1113, https://doi.org/10.1617/s11527-014-0274-y.
[31] C.A. Graubner, E. Boska, C. Motzko, T. Proske, F. Dehn, Formwork pressure induced by highly flowable concretes–design approach and transfer into practice, Struct. Concr. 13 (1) (2012) 51–60, https://doi.org/10.1002/suco.201100012.
[32] W. Brameshuber, H. Beitzel, M. Beitzel, C. Bohnemann, E. Boska, F. Dehn, C. A. Graubner, A. König, C. Motzko, H.S. Müller, K. Pistol, Formwork pressure induced by highly flowable concretes–material investigations and large-scale tests, Struct. Concr. 12 (4) (2011) 270–280, https://doi.org/10.1002/suco.201000013.
[33] J.D. Henschen, D.I. Castaneda, D.A. Lange, Formwork pressure model for self-consolidating concrete using pressure decay signature, ACI Mater. J. 115 (3) (2018) 339–348, https://doi.org/10.14359/51702183.
[34] M.A. Glinicki, J. Gołaszewski, G. Cygan, Formwork pressure of a heavyweight self-compacting concrete mix, Materials 14 (6) (2021) 1549, https://doi.org/10.3390/ma14061549.
[35] T. Proske, C.A. Graubner, Formwork pressure of highly workable concrete–experiments focused on setting, vibration and design approach, in: Design, Production and Placement of Self-Consolidating Concrete, Springer, 2010, pp. 255–267, https://doi.org/10.1007/978-90-481-9664-7_22.
[36] J.J. Assaad, J. Harb, Formwork pressure of self-consolidating concrete containing recycled coarse aggregates, ACI Mater. J. 114 (3) (2017), https://doi.org/10.14359/51689494.

[37] A.F. Omran, K.H. Khayat, Portable pressure device to evaluate lateral formwork pressure exerted by fresh concrete, J. Mater. Civ. Eng. 25 (6) (2013) 731–740, https://doi.org/10.1061/(ASCE)MT.1943-5533.0000537.
[38] P. Ghoddousi, A.A. Shirzadi Javid, G. Ghodrati Amiri, K. Donyadideh, Predicting the formwork lateral pressure of self-consolidating concrete based on experimental thixotropy values, Int. J. Civil Eng. 17 (7) (2019) 1131–1144, https://doi.org/10.1007/s40999-018-0368-y.
[39] P. Shakor, N. Gowripalan, Pressure exerted on formwork and early age shrinkage of self- technical papers pressure exerted on formwork and early age shrinkage of self-compacting concrete, Concrete in Australia (2020), https://doi.org/10.1016/j.cscm.2021.e00642.
[40] G.R. Lomboy, X. Wang, K. Wang, Rheological behavior and formwork pressure of SCC, SFSCC, and NC mixtures, Cem. Concr. Compos. 54 (2014) 110–116, https://doi.org/10.1016/j.cemconcomp.2014.05.001.
[41] S. Teixeira, I. Puente, A. Santilli, Statistical model for predicting the maximum lateral pressure exerted by self-consolidating concrete on vertical formwork, J. Build. Eng. 12 (2017) 77–86, https://doi.org/10.1016/j.jobe.2017.05.004.
[42] J. Assaad, K.H. Khayat, H. Mesbah, Variation of formwork pressure with thixotropy of self-consolidating concrete, Dent. Mater. J. 100 (1) (2003) 29–37, https://doi.org/10.14359/12460.
[43] Y. Gamil, J. Nilimaa, M. Emborg, A. Cwirzen, Lateral formwork pressure for self-compacting concrete—a review of prediction models and monitoring technologies, Materials 14 (16) (2021) 4767, https://doi.org/10.3390/ma14164767.
[44] P.H. Billberg, N. Roussel, S. Amziane, M. Beitzel, G. Charitou, B. Freund, J. N. Gardner, G. Grampeix, C.A. Graubner, L. Keller, K.H. Khayat, Field validation of models for predicting lateral form pressure exerted by SCC, Cem. Concr. Compos. 54 (2014) 70–79, https://doi.org/10.1016/j.cemconcomp.2014.02.003.
[45] P.G. Asteris, A.D. Skentou, A. Bardhan, P. Samui, K. Pilakoutas, Predicting concrete compressive strength using hybrid ensembling of surrogate machine learning models, Cem. Concr. Res. 145 (2021), 106449, https://doi.org/10.1016/j.cemconres.2021.106449.
[46] J.J. Assaad, P. Matar, Regression models to predict SCC pressure exerted on formworks containing vertical and transverse reinforcing bars, Mater. Struct. 51 (3) (2018) 1–18, https://doi.org/10.1617/s11527-018-1188-x.
[47] G. Ovarlez, N. Roussel, A physical model for the prediction of lateral stress exerted by self-compacting concrete on formwork, Mater. Struct. 39 (2) (2006) 269–279, https://doi.org/10.1617/s11527-005-9052-1.
[48] M. Beitzel, Modeling fresh concrete pressure of normal and self-compacting concrete, in: Design, Production and Placement of Self-Consolidating Concrete, Springer, 2010, pp. 243–254, https://doi.org/10.1007/978-90-481-9664-7_21.
[49] R. Mitchell, J. Michalski, T. Carbonell, An Artificial Intelligence apprOach, Springer, 2013, https://doi.org/10.1002/zamm.19850651113.
[50] J.A. Guzmán-Torres, F.J. Domínguez-Mota, E.M. Alonso-Guzmán, Estimating the flexural strength of concrete using compressive strength as input value in a deep learning model, in: IOP Conference Series: Materials Science and Engineering, IOP Publishing, 2021, https://doi.org/10.1088/1757-899X/1150/1/012019/meta.
[51] H. Tanyildizi, A. Şengür, Y. Akbulut, M. Şahin, Deep learning model for estimating the mechanical properties of concrete containing silica fume exposed to high temperatures, Front. Struct. Civ. Eng. 14 (6) (2020) 1316–1330, https://doi.org/10.1007/s11709-020-0646-z.
[52] M. Nasrollahi, N. Bolourian, A. Hammad, Concrete surface defect detection using deep neural network based on lidar scanning, in: Proceedings of the CSCE Annual Conference, Laval, Greater Montreal, QC, Canada, 2019. https://www.researchgate.net/publication/335276365_Concrete_Surface_Defect_Detection_Using_Deep_Neural_Network_Based_on_LiDAR_Scanning.
[53] C. Kina, K. Turk, E. Atalay, I. Donmez, H. Tanyildizi, Comparison of extreme learning machine and deep learning model in the estimation of the fresh properties of hybrid fiber-reinforced SCC, Neural Comput. & Applic. 33 (18) (2021) 11641–11659, https://doi.org/10.1007/s00521-021-05836-8.
[54] K.T. Nguyen, Q.D. Nguyen, T.A. Le, J. Shin, K. Lee, Analyzing the compressive strength of green fly ash based geopolymer concrete using experiment and machine learning approaches, Constr. Build. Mater. 247 (2020), 118581, https://doi.org/10.1016/j.conbuildmat.2020.118581.
[55] O.R. Abuodeh, J.A. Abdalla, R.A. Hawileh, Assessment of compressive strength of ultra-high performance concrete using deep machine learning techniques, Appl. Soft Comput. 95 (2020), 106552, https://doi.org/10.1016/j.asoc.2020.106552.
[56] F. Deng, Y. He, S. Zhou, Y. Yu, H. Cheng, X. Wu, Compressive strength prediction of recycled concrete based on deep learning, Constr. Build. Mater. 175 (2018) 562–569, https://doi.org/10.1016/j.conbuildmat.2018.04.169.
[57] H.B. Ly, T.A. Nguyen, V.Q. Tran, Development of deep neural network model to predict the compressive strength of rubber concrete, Constr. Build. Mater. 301 (2021), 124081, https://doi.org/10.1016/j.conbuildmat.2021.124081.
[58] T. Nguyen, A. Kashani, T. Ngo, S. Bordas, Deep neural network with high-order neuron for the prediction of foamed concrete strength, Comput. Aid. Civil Infrastruct. Eng. 34 (4) (2019) 316–332, https://doi.org/10.1111/mice.12422.
[59] J. Deng, Y. Lu, V.C.S. Lee, Concrete crack detection with handwriting script interferences using faster region-based convolutional neural network, Comput. Aid. Civil Infrastruct. Eng. 35 (4) (2020) 373–388, https://doi.org/10.1111/mice.12497.
[60] A.T. Huynh, Q.D. Nguyen, Q.L. Xuan, B. Magee, T. Chung, K.T. Tran, K.T. Nguyen, A machine learning-assisted numerical predictor for compressive strength of geopolymer concrete based on experimental data and sensitivity analysis, Appl. Sci. 10 (21) (2020) 7726, https://doi.org/10.3390/app10217726.
[61] V. Tra, T.K. Nguyen, C.H. Kim, J.M. Kim, Health indicators construction and remaining useful life estimation for concrete structures using deep neural networks, Appl. Sci. 11 (9) (2021) 4113, https://doi.org/10.3390/app11094113.
[62] P.N. Pizarro, L.M. Massone, Structural design of reinforced concrete buildings based on deep neural networks, Eng. Struct. 241 (2021), 112377, https://doi.org/10.1016/j.engstruct.2021.112377.
[63] H. Naderpour, A.H. Rafiean, P. Fakharian, Compressive strength prediction of environmentally friendly concrete using artificial neural networks, J. Build. Eng. 16 (2018) 213–219, https://doi.org/10.1016/j.jobe.2018.01.007.
[64] T. Han, A. Siddique, K. Khayat, J. Huang, A. Kumar, An ensemble machine learning approach for prediction and optimization of modulus of elasticity of recycled aggregate concrete, Constr. Build. Mater. 244 (2020), 118271, https://doi.org/10.1016/j.conbuildmat.2020.118271.
[65] V.Q. Tran, V.Q. Dang, L.S. Ho, Evaluating compressive strength of concrete made with recycled concrete aggregates using machine learning approach, Constr. Build. Mater. 323 (2022), 126578, https://doi.org/10.1016/j.conbuildmat.2022.126578.
[66] I. Nunez, M.L. Nehdi, Machine learning prediction of carbonation depth in recycled aggregate concrete incorporating SCMs, Constr. Build. Mater. 287 (2021), 123027, https://doi.org/10.1016/j.conbuildmat.2021.123027.
[67] Z.H. Duan, S.C. Kou, C.S. Poon, Prediction of compressive strength of recycled aggregate concrete using artificial neural networks, Constr. Build. Mater. 40 (2013) 1200–1206, https://doi.org/10.1016/j.conbuildmat.2012.04.063.
[68] S. Yokoyama, T. Matsumoto, Development of an automatic detector of cracks in concrete using machine learning, Proc. Eng. 171 (2017) 1250–1255, https://doi.org/10.1016/j.proeng.2017.01.418.
[69] M. Słoński, K. Schabowicz, E. Krawczyk, Detection of flaws in concrete using ultrasonic tomography and convolutional neural networks, Materials 13 (7) (2020) 1557, https://doi.org/10.3390/ma13071557.
[70] Y. Gamil, A. Cwirzen, Digital transformation of concrete technology—a review, Front. Built Environ. (2022) 8, https://doi.org/10.3389/fbuil.2022.835236.
[71] A. Perrot, A. Pierre, S. Vitaloni, V. Picandet, Prediction of lateral form pressure exerted by concrete at low casting rates, Mater. Struct. 48 (7) (2015) 2315–2322, https://doi.org/10.1617/s11527-014-0313-8.
[72] N. Baldo, J. Valentin, E. Manthos, M. Miani, Numerical characterization of high modulus asphalt concrete containing rap: a comparison among optimized shallow neural models, in: IOP Conference Series: Materials Science and Engineering, IOP Publishing, 2020, https://doi.org/10.1088/1757-899X/960/2/022083.
[73] P.G. Asteris, V.G. Mokos, Concrete compressive strength using artificial neural networks, Neural Comput. & Applic. 32 (15) (2020) 11807–11826, https://doi.org/10.1007/s00521-019-04663-2.
[74] H.C. Tsai, Predicting strengths of concrete-type specimens using hybrid multilayer perceptrons with center-unified particle swarm optimization, Expert Syst. Appl. 37 (2) (2010) 1104–1112, https://doi.org/10.1016/j.eswa.2009.06.093.
[75] C.A. Jeyasehar, K. Sumangala, Damage assessment of prestressed concrete beams using artificial neural network (ANN) approach, Comput. Struct. 84 (26–27) (2006) 1709–1718, https://doi.org/10.1016/j.compstruc.2006.03.005.
[76] A.K. Pani, H.K. Mohanta, Online monitoring and control of particle size in the grinding process using least square support vector regression and resilient back propagation neural network, ISA Trans. 56 (2015) 206–221, https://doi.org/10.1016/j.isatra.2014.11.011.
[77] J.I. Kim, D.K. Kim, M.Q. Feng, F. Yazdani, Application of neural networks for estimation of concrete strength, J. Mater. Civ. Eng. 16 (3) (2004) 257–264, https://doi.org/10.1007/BF02841997.
[78] Y. Yu, K. Adu, N. Tashi, P. Anokye, X. Wang, M.A. Ayidzoe, Rmaf: Relu-memristor-like activation function for deep learning, IEEE Access 8 (2020) 72727–72741. https://ieeexplore.ieee.org/iel7/6287639/8948470/09066950.pdf.
[79] N. Ketkar, N. Ketkar, Stochastic gradient descent, in: Deep Learning with Python, Springer, 2017, pp. 113–132, https://doi.org/10.1007/978-1-4842-2766-4_8.
[80] P. Toulis, D. Tran, E. Airoldi, Towards stability and optimality in stochastic gradient descent, in: Artificial Intelligence and Statistics, PMLR, 2016, in: https://proceedings.mlr.press/v51/toulis16.html.
[81] T. Najeh, J. Lundberg, A. Kerrouche, Deep-learning and vibration-based system for Wear size estimation of railway switches and crossings, Sensors 21 (15) (2021) 5217, https://doi.org/10.3390/s21155217.
[82] A. Sherstinsky, Fundamentals of recurrent neural network (RNN) and long short-term memory (LSTM) network, Physica D: Nonlinear Phenomena 404 (2020), 132306, https://doi.org/10.1016/j.physd.2019.132306.
[83] H. Wang, C. Ma, L. Zhou, A brief review of machine learning and its application, in: 2009 *International Conference on Information Engineering and Computer Science*, IEEE, 2009. https://ieeexplore.ieee.org/document/5362936.
[84] J. Wang, Y. Zou, P. Lei, R.S. Sherratt, L. Wang, Research on recurrent neural network based crack opening prediction of concrete dam, J. Internet Technol. 21 (4) (2020) 1161–1169. https://jit.ndhu.edu.tw/article/view/2343/2357.
[85] R.A. Rajagukguk, R.A. Ramadhan, H.J. Lee, A review on deep learning models for forecasting time series data of solar irradiance and photovoltaic power, Energies 13 (24) (2020) 6623, https://doi.org/10.3390/en13246623.
[86] G. Van Houdt, C. Mosquera, G. Nápoles, A review on the long short-term memory model, Artif. Intell. Rev. 53 (8) (2020) 5929–5955, https://doi.org/10.1007/s10462-020-09838-1.
[87] S. Shalev-Shwartz, S. Ben-David, Understanding Machine Learning: From Theory to Algorithms, Cambridge University Press, 2014. https://www.cs.huji.ac.il/~shais/UnderstandingMachineLearning/.

[88] J. Bergstra, Y. Bengio, Random search for hyper-parameter optimization, J. Mach. Learn. Res. 13 (2) (2012).
[89] I.K.M. Jais, A.R. Ismail, S.Q. Nisa, Adam optimization algorithm for wide and deep neural network, Knowl. Eng. Data Sci. 2 (1) (2019) 41–46, https://doi.org/10.17977/um018v2i12019p41-46.
[90] Y. Gamil, J. Nilimaa, A. Cwirzen, M. Emborg, Experimental based assessment of formwork pressure theoretical design models for self-compacting concrete, J. Build. Eng. 68 (2023), 106085.